Control Strategy for Grid-Connected Three-Phase Inverters During Voltage Sags to Meet Grid Codes and to Maximize Power Delivery Capability

Miguel Andrés Garnica López, Luis García de Vicuña, Jaume Miret, *Member*, *IEEE*, Miguel Castilla, and Ramón Guzmán

***Abstract*—Inverter-based distributed generation plays a vital role in the stability and reliability of new power systems. Under voltage sags, these systems must remain connected to the electrical network according to the stringent requirements of grid codes. Low-voltage ride-through control strategies are becoming a common trend in power electronics research. However, previous studies of these control strategies have not dealt with the different possible scenarios presented by new grid codes, and many of them focus on a very limited number of control objectives. In this study, an algorithm to maximize the converter capabilities was developed and subjected to experimental tests during different voltage sags. In this research, based on unbalanced voltage drops of several severity levels, six different cases of current injection are identified while taking into consideration the restrictions imposed by grid codes. The research results represent a further step towards the development of flexible controllers adaptable to the environments of intelligent electricity grids with high integration of distributed generation.**

***Index Terms*—Active power control, distributed power generation, grid code, low-voltage ride-through, maximum rated current, reactive power control, voltage sag.**

I. Introduction

NOWADAYS, problems associated with rapid growth of energy demand are worldwide recognized. Concepts such as energy transition, reliable energy supply, sustainable energy resources, and low environmental footprint are central to current research, and they represent a significant challenge, not only for scientists but also for politics and business [1].

Recent trends in clean energies have led to a large-scale proliferation of inverter-based distributed power generation systems (DPGSs) [2]. More recently, there has been a surge of interest in trying to ensure the stability and reliability of the electrical network by implementing increasingly stringent grid codes (GCs). These, in essence, set minimums that must be met for the sake of the security of the electrical infrastructure, especially under fault conditions [3]–[5].

Voltage sags are the principal power quality concern for process industries [6]. A voltage sag is a decrease in the rms voltage, typically between 0.1 p.u. and 0.9 p.u., for a period of 0.5 cycles to 1 minute [7]. This electromagnetic phenomenon is considered as a short-duration voltage variation, which is almost always caused by fault conditions. Hence, to make distributed generation (DG) systems behave as much as possible in the same way as conventional power plants during faults, GCs typically require: 1) to do not disconnect from the grid, 2) to support the voltage recovery by injecting reactive current, and 3) resuming active power supply after the fault clearance [8]–[10].

Evidence suggests that low-voltage ride-through (LVRT) capability is the most important requirement for maintaining network integrity and it is defined as a voltage-against-time profile at the connection point for fault conditions. It describes the conditions in which the source must remain connected to the utility grid, operating steadily after the electrical system has been disturbed by secured faults [11]. Concerning the reactive current injection capability, the GCs provide the curve that relates the percentage of reactive current to be injected as a function of the voltage at the point of common coupling (PCC) [12]–[15]. On three-phase faults, the LVRT capability is explicitly specified by GCs, but in the case of asymmetrical faults, this capability will be defined by each transmission system operator (TSO) [16]. Because of that, the method of symmetrical components provides a practical tool for analyzing and understanding the operation of a system during unbalanced conditions, taking into account that asymmetrical faults have a very high percentage of occurrence (97%–98%) [17].

During the last decade, different control strategies have been presented to improve the performance of the inverter during grid faults and to guarantee power delivery to loads during a short-term voltage drop [18]–[31], most of them based on symmetrical components since their use allow

Manuscript received Month xx, 2xxx; revised Month xx, xxxx; accepted Month x, xxxx. This work has been supported by the European Union Project ELAC2014/ESE0034, and it is linked to Spanish National Project PCIN-2015-001 and also supported by the Ministry of Economy and Competitiveness of Spain under project ENE2015-64087-C2-1-R. Recommended for publication by Associate Editor xxxx.

Miguel A. Garnica L. is with the Grupo de Investigación en Comunicación, Control y Diseño Naval, Escuela Naval de Cadetes “Almirante Padilla”, Cartagena de Indias, D. T. y C. (Bolívar), Colombia, and with the Department of Electronic Engineering, Technical University of Catalonia, Av. Víctor Balaguer 1, Vilanova i la Geltrú, 08800, Spain (e-mail: miguel.garnica@armada.mil.co).

José L. García de Vicuña, Miguel Castilla Fernández, and Jaume Miret are with the Department of Electronic Engineering, Technical University of Catalonia, Av. Víctor Balaguer 1, Vilanova i la Geltrú, 08800, Spain (e-mail: vicuna@eel.upc.edu; miquel.castilla@upc.edu; jaume.miret@upc.edu).

Ramón Guzmán is with the Department of Automatic Control, Technical University of Catalonia, Av. Víctor Balaguer 1, Vilanova i la Geltrú, 08800, Spain (e-mail: ramon. guzman@upc.edu).

achieving different control objectives. In [18] different controllers are compared, and it is shown that they all meet LVRT requirements, but all control objectives cannot be achieved at the same time. In both [18], [19] and [24]–[26] it can be seen that each control strategy determines the degree of power quality delivered to the network. Other strategies have focused on reactive power injection to provide voltage support when balanced and unbalanced failures occur [20]–[22].

Several studies have documented the maximum current control to avoid the disconnection of the DG source due to overcurrent, as presented in [23]–[27]. However, these strategies have some drawbacks. In [23] the percentage of harmonic distortion increases. In [24], [25] active power cannot be injected under unbalanced faults. Under severe failures, the reference currents of the controller [26] may exceed the current capability of the inverter. In [27], the delivered power shows undesired oscillations.

Recent articles focusing on this research area (e.g., [28]–[31]) incorporate new algorithms considering certain specific techniques to maximize some power capabilities of the inverter. The control strategy proposed in [28] includes a sophisticated reference current generator that allows injecting active and reactive power through positive and negative sequences. However, the control algorithm is rather complex compared with previous conventional schemes. Specifically, [29] focuses on distributed photovoltaic (PV) systems giving priority to active power delivery to achieve maximum current injection. However, it considers neither any current GC nor the fact that, for instance, all German PV systems must have the capability to provide reactive power since 2011, following technical guidelines [32]. In [30], the E.ON code is applied, but the control strategy focuses on the maximum power point tracking (MPPT) of the boost converter for PV power systems. Two GCs are tested in [31], but the proposed method cannot avoid oscillations in the active power when only reactive current is injected into the network. On the contrary, the control strategy proposed in this work is relevant for any DPGS and it gives priority to reactive power injection, as established by current GCs. Moreover, injection of only reactive current is carried out without active power oscillations.

Control strategies should be optimized according to new GC requirements, taking into account not only performance and reliability considerations but also the opportunity offered by technological development to support an increasingly dynamic electrical network [33], [34]. In this sense, this paper presents an enhanced LVRT control strategy that introduces a new algorithm to meet four control objectives at the same time and, in this way, guarantee an optimum use of the power capabilities of the inverter. The objectives, formulated in hierarchical order, are 1) to meet GC requirements, 2) to limit current amplitude to the maximum value allowed by the inverter, 3) to perform active power control, and 4) to eliminate active power oscillations.

Many studies have similar objectives, but in previous works [20]–[26], only few control objectives can be accomplished simultaneously, as can be seen in Table V. Unlike, the proposed approach allows a better optimization of the power delivery by the inverters. Attempting to reach several control objectives at the same time not only involves addressing a different problem, but also the development of new control algorithms. In addition, the selection of the four objectives and the interaction among them during voltage sags improve the operation of these systems. These interactions have not been reported previously in the literature.

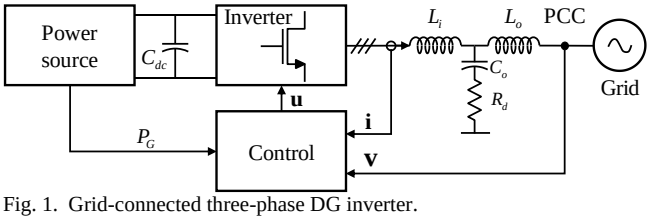

Fig. 1. Grid-connected three-phase DG inverter.

This paper has been organized into five sections. Section I provides a brief overview of the state of the art in LVRT control strategies of inverter-based DPGSs. Section II reviews the behavior of the grid-connected inverter under voltage sags. Section III deals with the formulated control objectives, the proposed control algorithm, and the chosen control scheme. In addition, a detailed discussion of the interactions among the control objectives during voltage sags is presented in this section. Section IV presents the findings of the research, focusing on selected experimental results that validate the proposal. Finally, Section V sets out some conclusions and it summarizes the main results of this paper.

II. Grid-Connected Inverters Under Voltage Sags

Inverters also known as power conditioning systems play a vital role in distributed resource (DR) applications [35]. Therefore, before proposing the objectives and the control algorithm, in this section, a description of the grid-connected voltage source inverter (VSI) under voltage sags is made. In addition, the basic requirements during these voltage disturbances and, specifically, the reactive current requirements adapted from the Spanish grid code are described.

A. Grid-Connected Three-Phase Inverter

Fig. 1 shows a simplified diagram of a distributed energy system connected to the network. The system includes the power source, a three-phase inverter, and the utility grid. A dc-link capacitor C_{dc} operates the interconnection between the power source and the inverter to balance the power flow [28], [29]. An external controller provides the generated active power reference (P_G) that should be injected into the grid. The current and voltage vectors (**i**, **v**) are sensed and supplied to the controller, which provides the control outputs (**u**). Finally, to obtain a grid-side current with a low harmonic content, a damped *LCL* filter is used at the inverter output [36].

B. Voltage Sag Characterization

During voltage sags, it is possible to describe the instantaneous phase voltages at the PCC as the addition of their positive- and negative-symmetric sequences [19], and these can be expressed in the $\alpha\beta$-frame by using Clarke's transformation, resulting in

$$v_\alpha = v_\alpha^+ + v_\alpha^- = V^+\cos(\omega t+\varphi)+V^-\cos(\omega t) \quad (1)$$

$$v_\beta = v_\beta^+ + v_\beta^- = V^+\sin(\omega t+\varphi)-V^-\sin(\omega t) \quad (2)$$

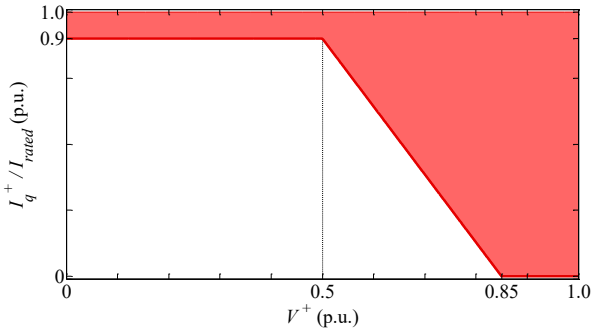

Fig. 2. Reactive current requirement adapted from the Spanish GC.

where v_α and v_β are the $\alpha\beta$-frame components, v_α^+, v_β^+, and v_α^-, v_β^- are the positive- and negative-sequence voltages, respectively. V^+ and V^- are the sequence amplitudes, ω is the grid angular frequency, and φ is the phase angle between positive and negative sequences, which is expressed as

$$\varphi = \cos^{-1}\left(\frac{v_\alpha^+ v_\alpha^- - v_\beta^+ v_\beta^-}{V^+ V^-}\right). \tag{3}$$

From the consideration of the sequence amplitude, the voltage unbalance factor (VUF) can be mathematically defined as the ratio of the V^- to the V^+ [37], [38]. Therefore:

$$\text{VUF} = \frac{V^-}{V^+} = \frac{\sqrt{\left(v_\alpha^-\right)^2 + \left(v_\beta^-\right)^2}}{\sqrt{\left(v_\alpha^+\right)^2 + \left(v_\beta^+\right)^2}}. \tag{4}$$

C. Reactive Current Requirements During Voltage Sags

Reactive current injection (RCI) during fault and recovery is required to minimize the voltage drop in the grid and to ensure a fast voltage recovery after the failure. Depending on the voltage at the PCC, the DPGS has to feed-in a certain reactive current [39]. This support improves the stability of the power system and it increases the quality and reliability of the network. The parameters of the RCI curve vary depending on the regulations of each country; however, efforts are being made to unify the criteria of this requirement.

The Spanish wind GC [13], used in this study and adapted as shown in Fig. 2, requires DG to supply the maximum possible current (I_{rated}) during fault periods, and it demands a reactive/rated current ratio between 0.5 p.u. and 0.85 p.u. of grid voltage sag. As soon as the PCC voltage is less than 0.5 p.u., the DG must be able to output at least 0.9 p.u. of reactive current.

Based on [17] and considering that this GC assumes only balanced faults, and therefore balanced currents, the axes of Fig. 2 have been renamed and identified only with their positive sequences to maximize the VSI power capabilities. The *x*-axis, PCC voltage in the GC, has been replaced by V^+ (the positive sequence voltage), and the *y*-axis, I_q / I_{total} in the GC, has been replaced by $I_q{}^+{}_{GC} = I_q^+ / I_{rated}$.

III. Proposed Control Objectives and Control Algorithm

This section formulates the control objectives to be achieved by the DPGS. It develops the mathematical expressions that allow fulfilling the proposed control objectives and, finally, it explains the control algorithm.

A. Control Objectives

This research focuses on an improved LVRT control strategy with a new control algorithm and four control objectives that are simultaneously addressed by the DPGS when a voltage sag occurs. These objectives are formulated and explained taking into account their hierarchy and priority in the proposed control algorithm:

1) To meet LVRT and RCI requirements defined in current GCs.
2) To limit the amount of injected current to the maximum allowed by the inverter.
3) Active power control in normal operation and under grid voltage sags.
4) To avoid active power oscillations.

1) Objective 1

The inverter must inject all the available current during the sag, i.e., I_{rated}, and meet RCI requirements set forth in Fig. 2:

$$I_{q\,GC}^+ = \begin{cases} 0.90 & \text{p.u., if } 0.00 \le V^+ \le 0.50 \text{ p.u.} \\ -k_1 V^+ + k_2 & \text{p.u., if } 0.50 < V^+ < 0.85 \text{ p.u.,} \\ 0.00 & \text{p.u., if } 0.85 \le V^+ \le 1.10 \text{ p.u.} \end{cases} \tag{5}$$

subject to

$$I_{q\,GC}^+ \le 1 \text{ p.u.} \tag{6}$$

where $I_q{}^+{}_{GC}$ is the minimum reactive current required by the GC during the voltage sag, being k_1 = 2.57 and k_2 = 2.19 the slope of the line defining the minimum RCI and the intersection with the *y*-axis, respectively.

2) Objective 2

To limit phase current amplitude to the maximum allowed by the inverter to operate safely:

$$\max\left\{I_a, I_b, I_c\right\} = I_{rated} \tag{7}$$

where I_a, I_b, and I_c are the phase current amplitudes. This protection always remains active; when the voltage drops, currents increase to maintain P_G.

3) Objective 3

Active power control in normal operation (V^+ > 0.85 p.u.) and under grid disturbances (V^+ < 0.85p.u.). Whenever it is possible, the purpose is to inject the maximum active power:

$$P^* = P_G \tag{8}$$

where P^* is the active power reference. When the outer P_G cannot be injected, due that I_{rated} is exceeded, active power curtailment (APC) will be applied. Active current injection, which is convenient from the source side, is essential to ensure power balance within the grid, and thus frequency stability [9], [10].

4) Objective 4

Whenever it is possible, the goal is to get the oscillating term of active power equal to zero to avoid oscillations at the dc-link, a desirable feature [40], that is why active and

reactive currents are required to be injected by positive and negative sequences. Therefore, the instantaneous active power (p) can be written as

$$p = P + \tilde{p} = P^* + 0 = P^* \quad (9)$$

where $\tilde{p}$ represents the oscillating term of the active power.

B. Scheme of Reference Currents

There are several schemes for generating reference currents [28]–[31]. Here, it has been chosen the scheme proposed in [29]. This scheme starts from two mathematical expressions defined as a function of the positive- and negative-sequence voltages, the sequence amplitudes, the power references, and four control parameters (k_p^+, k_p^-, k_q^+, and k_q^-) used to balance the positive and negative sequences:

$$i_\alpha^* = \frac{2}{3}\left(\left(\frac{\left(k_p^+ v_\alpha^+ + k_p^- v_\alpha^-\right)P^*}{k_p^+\left(V^+\right)^2 + k_p^-\left(V^-\right)^2}\right) + \left(\frac{\left(k_q^+ v_\beta^+ + k_q^- v_\beta^-\right)Q^*}{k_q^+\left(V^+\right)^2 + k_q^-\left(V^-\right)^2}\right)\right) \quad (10)$$

$$i_\beta^* = \frac{2}{3}\left(\left(\frac{\left(k_p^+ v_\beta^+ + k_p^- v_\beta^-\right)P^*}{k_p^+\left(V^+\right)^2 + k_p^-\left(V^-\right)^2}\right) - \left(\frac{\left(k_q^+ v_\alpha^+ + k_q^- v_\alpha^-\right)Q^*}{k_q^+\left(V^+\right)^2 + k_q^-\left(V^-\right)^2}\right)\right) \quad (11)$$

where Q^* is the reactive power reference. It is noteworthy to mention that the control parameters have been selected as [29] $k_p^- = -k_p^+$ and $k_q^+ = k_q^-$ to eliminate the active power oscillations.

An appropriate set of reference currents is needed to achieve the proposed control objectives. By developing (10) and (11), the reference current generator can be formulated using four variables that indicate the amplitude of the positive- and negative-sequence currents associated with the active and reactive powers (I_p^+, I_p^-, I_q^+, and I_q^-).

The reference currents are constructed with these variables and the normalized positive- and negative-sequence voltages (v^+ / V^+, v^- / V^-). The first variables generate the current amplitudes and the last ones, the current waveforms that allow injecting active and reactive powers via positive and negative sequences. These reference currents can be written as follows:

$$i_\alpha^* = I_p^+\left(\frac{v_\alpha^+}{V^+}\right) - I_p^-\left(\frac{v_\alpha^-}{V^-}\right) + I_q^+\left(\frac{v_\beta^+}{V^+}\right) + I_q^-\left(\frac{v_\beta^-}{V^-}\right) \quad (12)$$

$$i_\beta^* = I_p^+\left(\frac{v_\beta^+}{V^+}\right) - I_p^-\left(\frac{v_\beta^-}{V^-}\right) - I_q^+\left(\frac{v_\alpha^+}{V^+}\right) - I_q^-\left(\frac{v_\alpha^-}{V^-}\right). \quad (13)$$

Note that voltage and reference currents are in phase for active power injection while they are 90º out-of-phase for reactive power injection.

The values of the four current amplitudes determine the performance of the system through the fulfillment of the control objectives:

1) The amplitude of the positive-sequence reactive current I_q^+ is directly related to GC compliance during fault conditions. Control of this variable allows objective 1 to be reached according to Fig. 2.
2) Objective 2 will be discussed in Section III-C.
3) The amplitude of the positive-sequence active current I_p^+ is calculated as (14):

$$I_p^+ = \frac{2}{3}\frac{V^+}{\left(V^+\right)^2 - \left(V^-\right)^2}P^*. \quad (14)$$

This expression allows the injection of active power into the grid during normal operation as well as in failure condition. Control of this variable allows reaching objective 3.

4) The negative-sequence components of active and reactive currents I_p^- and I_q^- are the variables associated with the elimination of the active power oscillations. These amplitudes can be written as:

$$I_p^- = \frac{V^-}{V^+}I_p^+ \quad (15)$$

$$I_q^- = \frac{V^-}{V^+}I_q^+. \quad (16)$$

Control of these variables is mandatory to achieve objective 4.

C. Current Amplitude Limitation Control

The maximum amplitude of each phase current can be obtained using (1), (2), (14)–(16) in (12), (13) and applying the inverse Clarke's transformation. The resulting amplitudes are a function of both the sag characteristics and the magnitudes of I_p^+ and I_q^+:

$$I_a = \sqrt{\frac{\left(V^+\right)^2 - 2V^+V^-\cos(\varphi) + \left(V^-\right)^2}{\left(V^+\right)^2}\left(\left(I_p^+\right)^2 + \left(I_q^+\right)^2\right)} \quad (17)$$

$$I_b = \sqrt{\frac{\left(V^+\right)^2 - 2V^+V^-\cos\left(\varphi - \frac{2\pi}{3}\right) + \left(V^-\right)^2}{\left(V^+\right)^2}\left(\left(I_p^+\right)^2 + \left(I_q^+\right)^2\right)} \quad (18)$$

$$I_c = \sqrt{\frac{\left(V^+\right)^2 - 2V^+V^-\cos\left(\varphi + \frac{2\pi}{3}\right) + \left(V^-\right)^2}{\left(V^+\right)^2}\left(\left(I_p^+\right)^2 + \left(I_q^+\right)^2\right)}. \quad (19)$$

From (17)–(19), it can be seen that the phase with the maximum current amplitude is the phase with the minimum value of the cosine function

$$x = \min\left\{\cos(\varphi),\ \cos\left(\varphi - \tfrac{2\pi}{3}\right),\ \cos\left(\varphi + \tfrac{2\pi}{3}\right)\right\}. \quad (20)$$

Then, the phase current maximum amplitude (I_{max}) can be calculated as

$$I_{\max} = \sqrt{\frac{\left(V^+\right)^2 - 2V^+V^-x + \left(V^-\right)^2}{\left(V^+\right)^2}\left(\left(I_p^+\right)^2 + \left(I_q^+\right)^2\right)}. \quad (21)$$

To avoid damage to the inverter or disconnection due to overcurrent, I_{max} must be limited to I_{rated}:

$$I_{\max} \le I_{rated}. \quad (22)$$

Equations (20)–(22) guarantee the fulfillment of control objective 2. Therefore, I_{max} will limit I_p^+ since I_q^+ is a value stipulated by the GC. Now the maximum amplitude of the positive-sequence active current can be calculated by using (21), $I_q^+ = I_q^+{}_{GC}$, $I_p^+ = I_p^+{}_{max}$, and $I_{max} = I_{rated}$. The resulting expression is solved for $I_p^+{}_{max}$:

$$I_{p\max}^{+}=\sqrt{\frac{\left(V^{+}\right)^{2}\left(I_{rated}\right)^{2}}{\left(V^{+}\right)^{2}-2V^{+}V^{-}x+\left(V^{-}\right)^{2}}-\left(I_{q\,GC}^{+}\right)^{2}} \tag{23}$$

which makes possible the fulfillment of control objective 3.

Taking into account the priority of reactive power injection during LVRT operation, I_p^+ must be limited to its maximum possible amplitude using the following condition:

$$I_p^+ \le I_{p\max}^+. \tag{24}$$

However, in a low-power production scenario, if I_p^+ were lower than $I_p^+{}_{max}$, the rated current of the inverter would not be reached. In this situation, the amplitude of the injected reactive current must be increased so that the inverter output current reaches I_{rated} to improve voltage support. The new amplitude of the positive-sequence reactive current can be directly calculated by using (21) and $I_{max} = I_{rated}$, and solving the resulting expression for I_q^+:

$$I_q^+=\sqrt{\frac{\left(V^{+}\right)^{2}\left(I_{rated}\right)^{2}}{\left(V^{+}\right)^{2}-2V^{+}V^{-}x+\left(V^{-}\right)^{2}}-\left(I_p^+\right)^{2}}. \tag{25}$$

Equations (5) and (25) guarantee the fulfillment of control objective 1.

D. Active Power Oscillations

According to [41], the instantaneous active and reactive powers delivered by a three-phase VSI can be defined as

$$p=\frac{3}{2}\left(v_\alpha i_\alpha + v_\beta i_\beta\right) \tag{26}$$

$$q=\frac{3}{2}\left(v_\beta i_\alpha - v_\alpha i_\beta\right). \tag{27}$$

Likewise, under unbalanced grid conditions, the instantaneous powers injected by the VSI can be decomposed in the following expressions:

$$p = p^+ + p^- + \tilde{p} \tag{28}$$

$$q = q^+ + q^- + \tilde{q} \tag{29}$$

where p^+, p^-, $\tilde{p}$, q^+, q^-, and $\tilde{q}$ represents the positive, negative and oscillatory terms of the active and reactive powers, respectively. Hence, by Inserting (1)–(2) and (10)–(11) into (26) and (27), (28) and (29) become functions of the voltage sag characteristics (V^+, V^-, and φ) and the control parameters (k_p^+, k_p^-, k_q^+, and k_q^-). Since it is the claimed objective, only the instantaneous active power is developed; details on the derivation of the reactive power oscillations can be found in [29]:

$$\begin{aligned} p=&\left[\frac{k_p^{+}\left(V^{+}\right)^{2}+k_p^{-}\left(V^{-}\right)^{2}}{k_p^{+}\left(V^{+}\right)^{2}+k_p^{-}\left(V^{-}\right)^{2}}P^{*}\right] \\ &+\left[\frac{\left(k_p^{+}+k_p^{-}\right)\left(V^{+}\right)\left(V^{-}\right)\cos\left(2wt-\varphi\right)}{k_p^{+}\left(V^{+}\right)^{2}+k_p^{-}\left(V^{-}\right)^{2}}P^{*}\right] \\ &+\left[\frac{\left(k_q^{+}-k_q^{-}\right)\left(V^{+}\right)\left(V^{-}\right)\sin\left(2wt-\varphi\right)}{k_q^{+}\left(V^{+}\right)^{2}+k_q^{-}\left(V^{-}\right)^{2}}Q^{*}\right]. \end{aligned} \tag{30}$$

As a result, oscillations of instantaneous active power are eliminated when the control parameters $k_p^- = -k_p^+$ and $k_q^+ = k_q^-$ are used. Hence, (30) becomes $p = P^*$.

E. Reactive Current Requirements Versus Capability of Active Current Injection

This section analyzes the basic conditions required to maximize the power capability of the inverter while meeting GCs. The amplitude of $I_q^+{}_{GC}$, determined by the GC, should be understood as a minimum value while the magnitude of $I_p^+{}_{max}$, given by (23), is the maximum current that can be injected to reach I_{rated}. It can be seen from the graphs in Fig. 3(a)–(b) how the amplitudes of $I_q^+{}_{GC}$ and $I_p^+{}_{max}$ change as a function of both V^+ and VUF variations. It can be said that to each pair of values of V^+ and VUF, there corresponds one and only one pair of values of $I_q^+ = I_q^+{}_{GC}$ and $I_p^+ = I_p^+{}_{max}$ and conversely.

In Fig. 3(a), observing at the front of the plane formed by the V^+ and $I_q^+{}_{GC}$ axes, it can be identified the plot of Fig. 2, which corresponds to the requirement of RCI when there is no imbalance, i.e., when VUF = 0. Therefore, for balanced grid faults, and according to (5), $I_q^+{}_{GC}$ increases when V^+ reduces from 0.85 p.u. and will not be less than 0.9 p.u. when V^+ is reduced from 0.5 p.u. Also, this current is always zero in the range $0.85 \le V^+ < 1$ p.u. since for this region there are no RCI requirements. As a result, it can be stated that multiple RCI curves are generated as the VUF increases from zero to its maximum value. The vertical plane located at $V^+ = 0.5$ p.u. shows how the injection of I_q^+ increases as the VUF increases: with VUF = 0.1, $I_q^+ = 0.9$ p.u. is required, but with VUF = 0.2, $I_q^+ = 1$ p.u. is mandatory. However, if the VUF increases much more, the injection of I_q^+ will reach its maximum value even for values of V^+ higher than 0.5 p.u., e.g., $I_q^+ = 1$ p.u. with $V^+ = 0.6$ p.u. and VUF = 0.8.

In Fig. 3(b), observing the back plane formed by the V^+ and $I_p^+{}_{max}$ axes, it can be seen the profile of $I_p^+{}_{max}$ injection when there is no imbalance, i.e., when VUF = 0. Therefore, for this condition, $I_p^+{}_{max}$ decreases when V^+ reduces from 0.85 p.u., but it will remain at 0.44 p.u. in the range $0.1 < V^+ \le 0.5$ p.u. The vertical plane located at $V^+ = 0.5$ p.u. shows how the injection of I_p^+ decreases as the VUF increases: with VUF = 0.1, it is possible to inject a current $I_p^+{}_{max} = 0.3$ p.u., but with VUF = 0.2, $I_p^+{}_{max} = 0$ p.u. is mandatory. However, if the VUF increases much more, the injection of $I_p^+{}_{max}$ will be null (zero) even for values of V^+ higher than 0.5 p.u., e.g., $I_p^+{}_{max} = 0$ with $V^+ = 0.6$ p.u. and VUF = 0.8. Note that $I_p^+{}_{max}$ is zero in the entire region to which the last point belongs. In this area, the injected reactive current I_q^+ is higher than $I_q^+{}_{GC}$ (a GC requirement) to supply the rated current once the active power is in the total curtailment region.

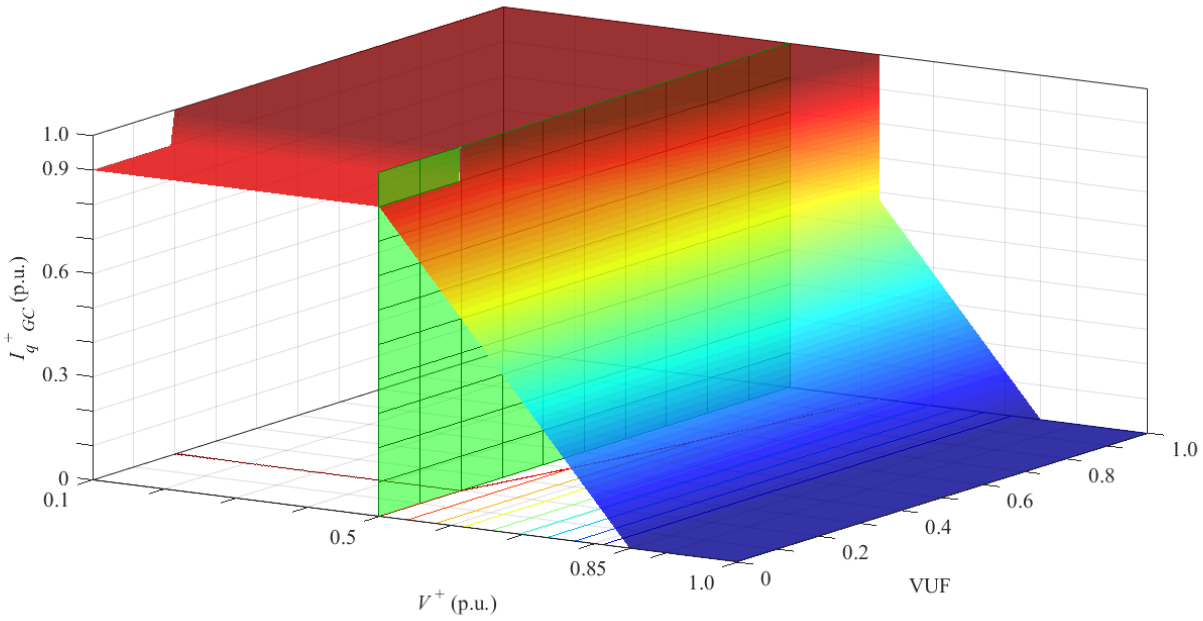

(a)

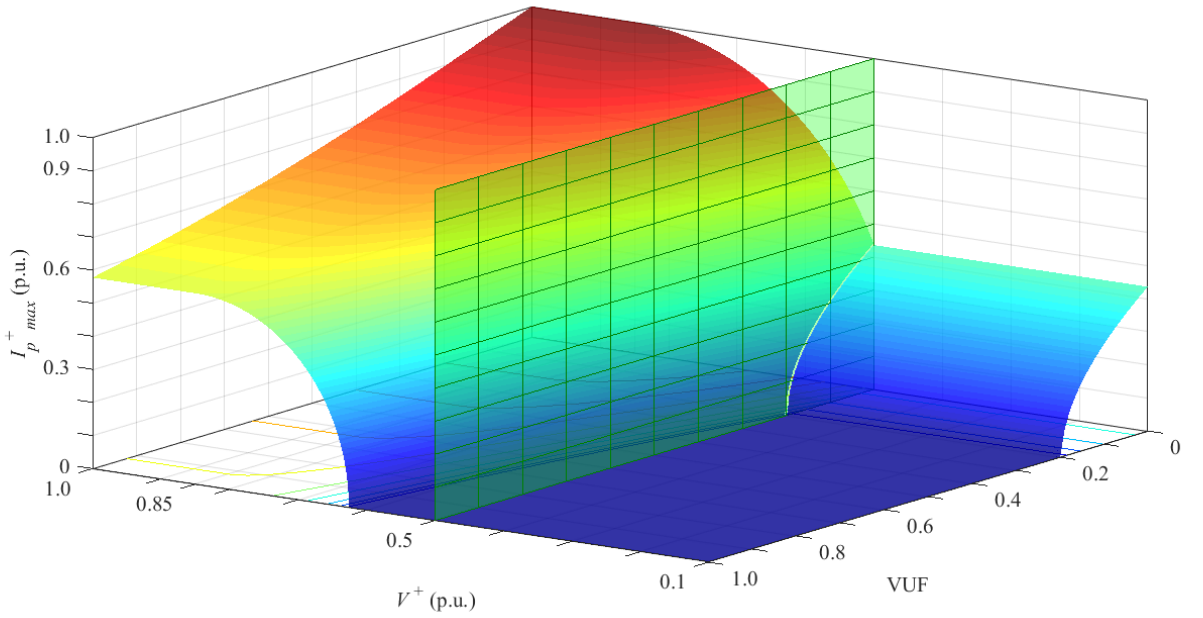

(b)

Fig. 3. Limits on positive-sequence active and reactive currents: (a) minimum positive-sequence reactive current injection I_q^+ and (b) maximum positive-sequence active current injection capability I_{p^+max}, as a function of the positive-sequence voltage (V^+) and the VUF.

Fig. 3 shows the degrees of freedom to choose the values of I_q^+ (always higher or equal to $I_q^+{}_{GC}$) and I_p^+ (always lower or equal to $I_p^+{}_{max}$). In addition, when an unbalanced sag occurs ($V^- > 0$), all the components of the active and reactive currents (I_p^+, I_p^-, I_q^+, and I_q^-) could be present. In contrast, when a balanced fault occurs ($V^- = 0$), only the positive sequence components (I_p^+ and I_q^+) will be present. It should be noted that (25) only applies when GC is met. Fig. 3 also shows that the capability of active current injection decreases when the RCI requirement increases and also when the fault is an unbalanced one. This behavior is due to the active power curtailment function in the control algorithm.

This previous analysis and the expressions obtained in Section III-C allow proposing a novel control algorithm which represents the main contribution of this work.

F. Control Algorithm

Fig. 4 shows the flowchart of the proposed control algorithm to determine the current amplitudes (I_p^+, I_p^-, I_q^+, and I_q^-) that will allow complying with the control objectives. Six different cases appear depending on the characteristics of the sag and the amount of generated active power. The flowchart

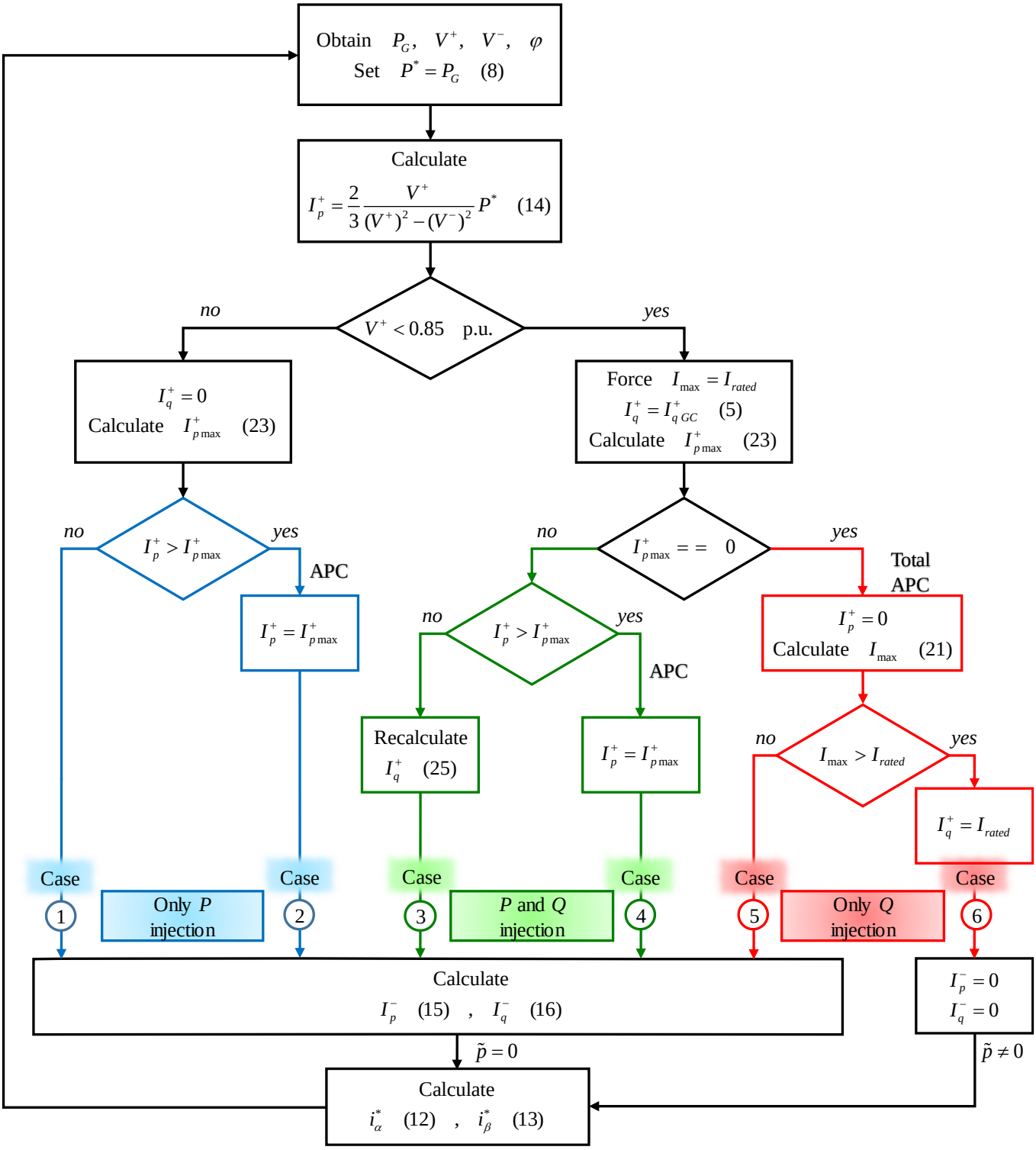

Fig. 4. Flowchart of the proposed control algorithm.

inputs are the generated active power (P_G), the measured voltage sequence amplitudes (V^+, V^-), and the sequence phase angle (φ). Initially, the active power reference is set as $P^* = P_G$ to calculate I_p^+ through (14) and to ensure that the maximum amount of active power will be injected (objective 3).

If there is no sag, as in cases 1 and 2 illustrated in blue on the left side of Fig. 4, (23) will be used to ensure that I_{max} is not exceeded (objective 2). Only if $I_p^+ > I_p^+{}_{max}$, active power curtailment is performed by setting $I_p^+ = I_p^+{}_{max}$. Note that, in this case, objective 2 predominates over objective 3, revealing the interaction between these two control objectives in the proposed control algorithm. On the other hand, the goal of avoiding active power oscillations (objective 4) is guaranteed with (15). In the first two cases there are no requirements for RCI ($I_q^+{}_{GC} = I_q^+ = I_q^- = 0$), and therefore, the inverter only delivers active power. In the four subsequent cases, when a voltage sag occurs ($V^+ < 0.85$ p.u.), there are requirements for RCI, and the inverter must inject its maximum current.

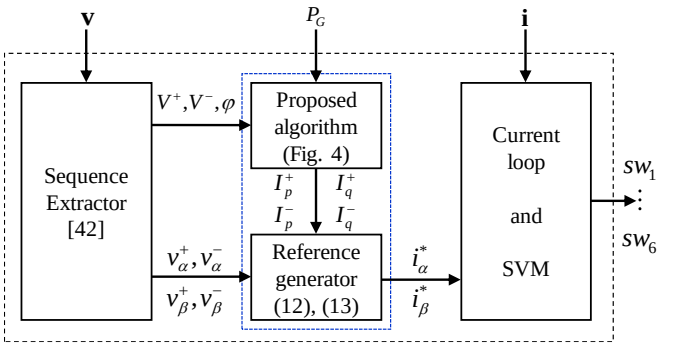

Fig. 5. Control diagram of the DG inverter.

In case of sag, I_q^+ is obtained from the GC (objective 1), and then (23) is used to know the corresponding $I_p^{+}{}_{max}$ value. For cases 3 and 4 shown in green on the central side of Fig. 4, all the components (I_p^+, I_p^-, I_q^+, and I_q^-) will be present. Particularly, in case 3, when the current I_p^+ does not exceed the limit $I_p^{+}{}_{max}$, then I_q^+ must be recalculated according to (25) . In this case, the value of I_q^+ from (23) will no longer be used, revealing the effect of objectives 2 and 3 over objective 1. For cases 5 and 6 shown in red on the right side of Fig. 4, the inverter only injects reactive current either by I_q^+ and I_q^- or only by I_q^+; therefore a total active power curtailment ($I_p^{+}{}_{max} = I_p^+ = I_p^- = 0$) is performed by the controller to avoid exceeding I_{rated}. The greatest interactions among control objectives appear in this part of the algorithm, as can be seen in Fig. 4. In particular, in case 6, all current components are updated through the algorithm. For instance, $I_q^- = 0$ to satisfy objective 2 as opposed to the value fixed by objective 4 with (16). These interactions have not been reported previously in the literature.

As expected, $I_q^+ = I_q^{+}{}_{GC}$ except when I_p^+ is lower than $I_p^{+}{}_{max}$ during voltage sags (fault conditions); in that case I_q^+ must be recalculated—according to (25)—to reach the maximum current capability of the inverter (I_{rated}). Likewise, when the voltage sag is very severe, and V^+ drops below 0.5 p.u., the inverter must deliver reactive power to the grid between 90% and 100% of its capability, according to the GC reference. Also, if V^- increases above a certain value, a total reduction of the active power will be mandatory. Equations (15) and (16) demonstrate that both I_p^- and I_q^- are proportional to the VUF and that they are a function of I_p^+ and I_q^+, respectively. Finally, the reference currents are calculated using (12) and (13).

G. Proposed Control Scheme

The proposed control scheme is shown in Fig. 5. The inputs of the controller are the measured phase voltages **v** at the PCC and the generated power P_G provided by the dc-link voltage controller. The voltage vector **v** is transformed into $\alpha\beta$-frame values by using Clarke's transformation. Then, voltages v_α and v_β are decomposed into symmetric components using a three-phase grid synchronization system [42]. The proposed algorithm block uses the outputs from the sequence extractor and P_G to calculate the amplitudes of the positive/negative sequence currents necessary to implement the reference currents, i_α^* and i_β^*. Finally, the duty cycles obtained from the current loops pass through a space vector modulator (SVM) to drive the switches of the inverter (sw_1 to sw_6).

TABLE I
EXPERIMENTAL PROTOTYPE PARAMETERS

Symbol	Quantity	Nominal value	
V	grid voltage	110.0	V rms
f	nominal grid frequency	60.0	Hz
S_b	rated power	2.3	kVA
I_{rated}	rated current amplitude	10.0	A
V_{dc}	dc-link voltage	400.0	V
C_{dc}	dc-link capacitor	1.0	mF
L_i	*LCL* inverter-side inductances	5.0	mH
C_o	*LCL* filter capacitors	2.0	μF
R_d	*LCL* damping resistors	68.0	Ω
L_o	*LCL* output-side inductances	2.0	mH
f_s	sampling/switching frequency	10.0	kHz

TABLE II
CHARACTERISTICS OF THE VOLTAGE SAGS

	PCC phase voltages (p.u.)			Sequence amplitudes (p.u.) and sequence phase angle		
Case	V_a	V_b	V_c	V^+	V^-	φ
1, 2	1.00	0.95	0.73	0.87	0.07	68°
3, 4	0.45	0.85	0.64	0.65	0.11	146°
5	0.50	0.35	0.50	0.45	0.05	57°
6	0.27	0.73	0.18	0.40	0.17	111°

TABLE III
ACTIVE AND REACTIVE POWER BEHAVIOR UNDER DIFFERENT VOLTAGE SAGS

	Generated power (W), averaged values p (W) and q (VAr), and peak value of active power oscillation (W)			
Case	P_G	p_{avg}	q_{avg}	$\tilde{p}$
1	1000	1000	0	0
2	2300	1868	0	0
3	700	700	1144	0
4	1400	1041	802	0
5	1400	0	957	0
6	1400	0	1102	430

TABLE IV
LABORATORY TEST RESULTS UNDER DIFFERENT VOLTAGE SAGS

	Current sequence amplitudes (A)					
Case	$I_q^{+}{}_{GC}$	I_q^+	I_q^-	$I_p^{+}{}_{max}$	I_p^+	I_p^-
1	0	0	0	9.26	4.96	0.40
2	0	0	0	9.26	9.26	0.75
3	5.14	7.33	1.24	7.06	4.75	0.80
4	5.14	5.14	0.87	7.06	7.06	1.20
5	9.00	9.00	1.00	0	0	0
6	9.00	10.00	0	0	0	0

IV. EXPERIMENTAL RESULTS

Considering Fig. 1, an experimental prototype rated at 2.3 kVA was built using a Guasch MTL-CBI0060F12IXHF full-bridge converter with an *LCL* filter for harmonic reduction [36]. A Texas Instruments F28M36 floating point DSP has been used as the control platform. The grid has been emulated using a programmable three-phase Pacific AMX-360 AC source, and the DG utilizing an AMREL SPS800-12-D013 DC source. The sequence extractor was implemented using second-order generalized integrators (SOGI) [42]. The current loops incorporate proportional-resonant controllers [43]. Table I shows the values of the main parameters of the experimental prototype.

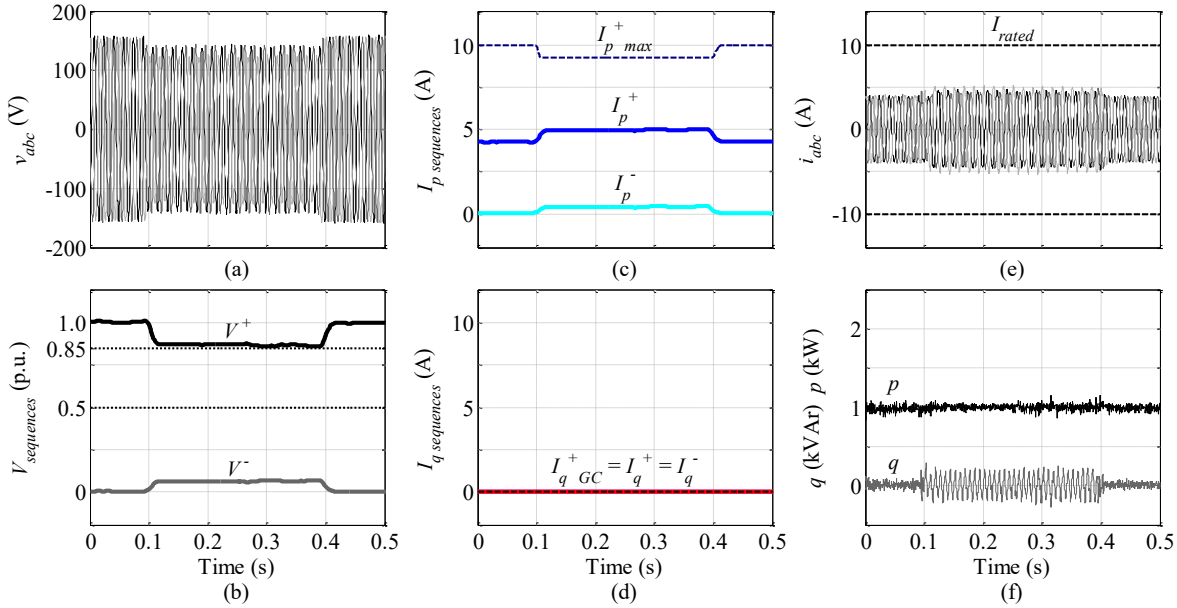

Fig. 6. Experimental results for case 1, only *P* injection without active power curtailment. (a) Phase voltages. (b) Voltage sequences. (c) Active current sequences. (d) Reactive current sequences. (e) Phase currents. (f) Measured powers.

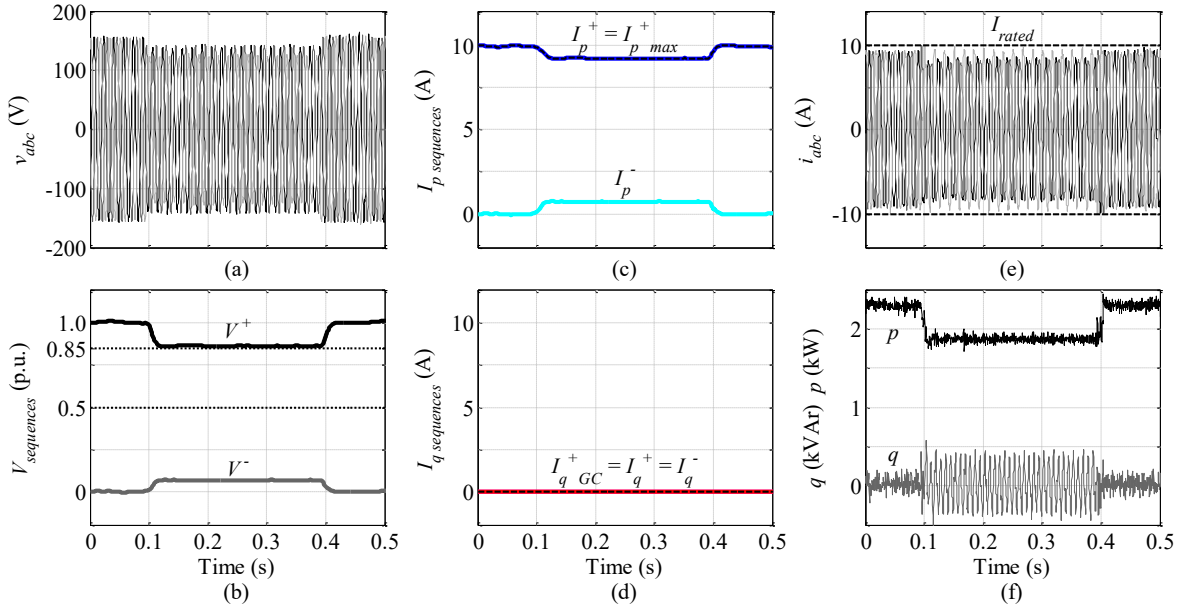

Fig. 7. Experimental results for case 2, only *P* injection with active power curtailment. (a) Phase voltages. (b) Voltage sequences. (c) Active current sequences. (d) Reactive current sequences. (e) Phase currents. (f) Measured powers.

All inverter variables are imported into MATLAB using a script which communicates the computer with the DSP. However, the active and reactive powers are calculated online within the DSP, in parallel while running the control algorithm.

Four different voltage faults were programmed in the AC source to evaluate the performance of the system under different voltage sag profiles (Table II) and different power references (Table III). All tests last 0.5 s, and each sag occurs from t = 0.1 s to t = 0.4 s. During this period, the behavior of the control strategy can be observed.In summary, Table IV consolidates the values of all the components (I_p^+, I_p^-, I_q^+, and I_q^-) obtained during each test, including those of $I_q{}^+{}_{GC}$ and $I_p{}^+{}_{max}$ to compare the cases.

The experimental results of each test are presented in the same figure with six subfigures ordered from left to right to show the evolution of each control action. Subfigures (a) and (b) point out the voltage sag. Subfigures (c) and (d) display the current amplitudes generated by the control algorithm. Finally, subfigures (e) and (f) present the system response through the phase currents and the delivered power. Note that the dotted black lines in (b) indicate the voltage thresholds of the GC, and the black dashed lines in (e) represent the maximum current that can be injected by the VSI according to its nominal ratings.

A. Case 1: Normal Operation and Low P_G

Fig. 6 displays the system in normal operation considering P_G = 1 kW (low-production scenario). Since V^+ > 0.85 p.u.

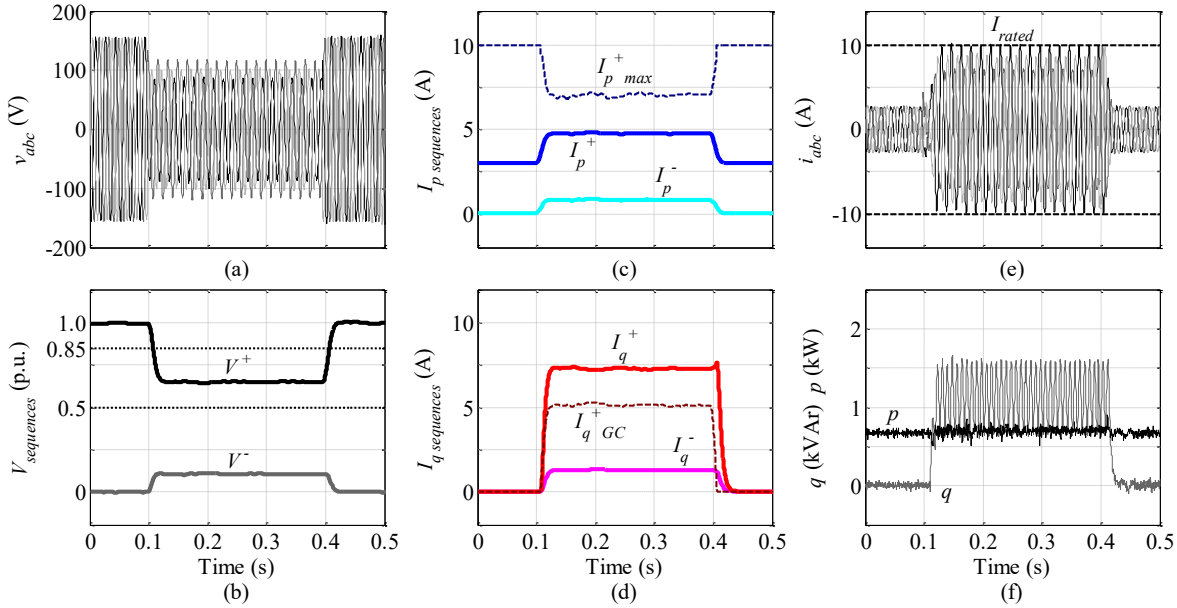

Fig. 8. Experimental results for case 3, *P* and *Q* injection without active power curtailment. (a) Phase voltages. (b) Voltage sequences. (c) Active current sequences. (d) Reactive current sequences. (e) Phase currents. (f) Measured powers.

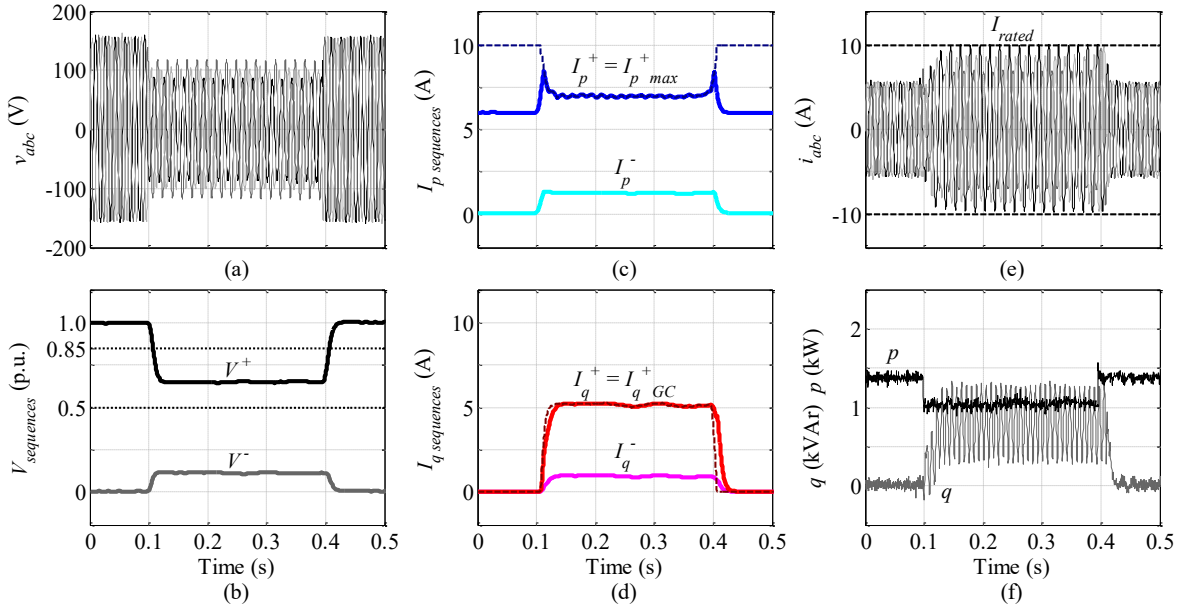

Fig. 9. Experimental results for case 4, *P* and *Q* injection with active power curtailment. (a) Phase voltages. (b) Voltage sequences. (c) Active current sequences. (d) Reactive current sequences. (e) Phase currents. (f) Measured powers.

then $I_q^+{}_{GC} = I_q^+ = I_q^- = 0$, and since $V^- > 0$ then the VSI injects active current through positive and negative sequences (I_p^+ and I_p^-). Also, $I_p^+ < I_p^+{}_{max}$, therefore $P^* = P_G$. It can be observed that the phase currents i_{abc} in Fig. 6(e) remain below the maximum allowable value (10 A) and that the delivered active power is maintained at a constant value of 1 kW without oscillations, as expected (objective 4). Obviously, reactive power presents oscillations that cannot be avoided.

B. Case 2: Normal Operation and High P_G

Fig. 7 shows the system in normal operation under the same voltage disturbance of the previous case, but considering P_G = 2.3 kW (high-production scenario). Observe that $I_p^+ = I_p^+{}_{max}$ = 9.26 A, therefore active power curtailment is performed during the sag (from 2.3 kW to 1.9 kW). As shown in Fig. 7(e), $i_c = I_{rated}$ (10 A) and the other phases remain below this value. Fig. 7(f) reveals that oscillations in the active power have also been avoided.

C. Case 3: Moderate Grid Fault Conditions and Low P_G

Fig. 8 shows the system in LVRT operation ($V^+ < 0.85$ p.u.) considering P_G = 700 W (low-production scenario). First, V^+ is equal to 0.65 p.u., and according to (5), the VSI has to inject into the grid a minimum reactive current $I_q^+{}_{GC}$ = 5.14 A. Secondly, with P_G = 700 W, the positive-sequence active current (I_p^+) is equal to 4.75 A. As a result, with these values of I_p^+ and $I_q^+{}_{GC}$, the rated current (I_{rated}) of the inverter is not reached and, therefore, the positive-sequence reactive current (I_q^+) is increased to 7.33 A by using (25). As can be seen in Fig. 8(e) and (f), the objective of injecting the maximum

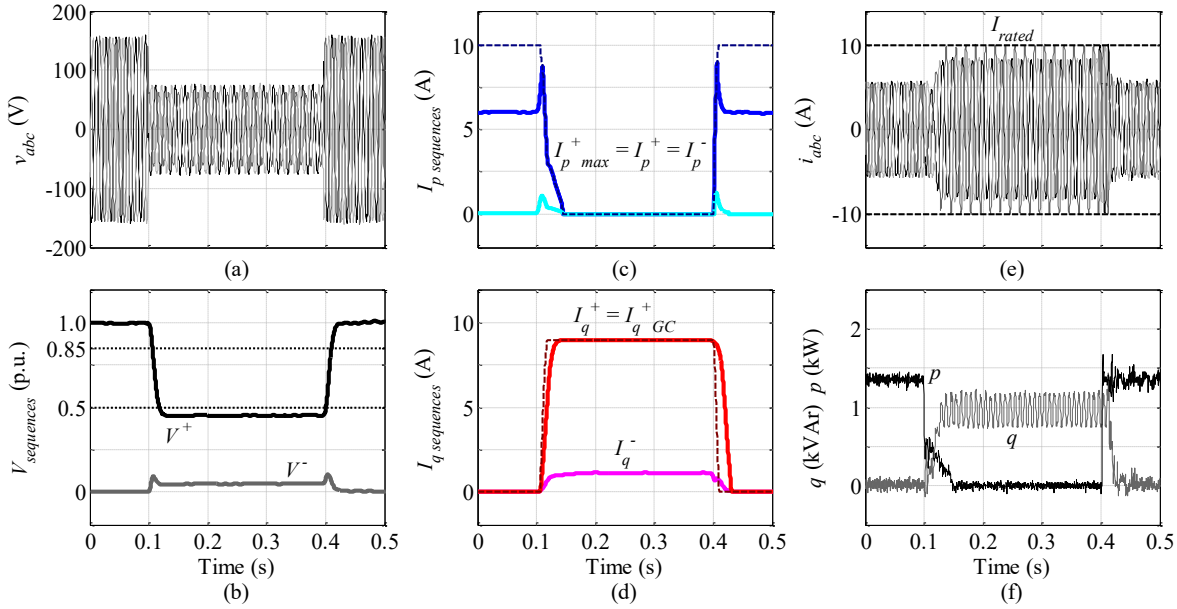

Fig. 10. Experimental results for case 5, only Q injection with full active power curtailment. (a) Phase voltages. (b) Voltage sequences. (c) Active current sequences. (d) Reactive current sequences. (e) Phase currents. (f) Measured powers.

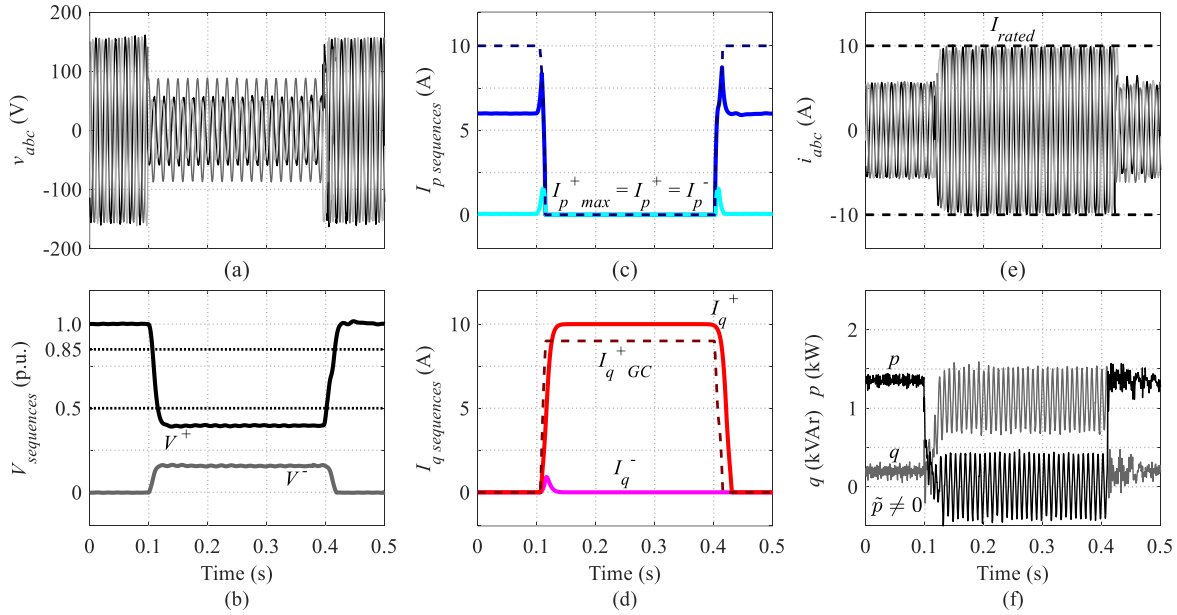

Fig. 11. Experimental results for case 6, only positive Q injection and full active power curtailment. (a) Phase voltages. (b) Voltage sequences. (c) Active current sequences. (d) Reactive current sequences. (e) Phase currents. (f) Measured powers.

allowed current is fulfilled, and the oscillating term of the active power is eliminated.

D. Case 4: Moderate Grid Fault Conditions and Medium P_G

Fig. 9 shows the system under the same sag of the previous case ($I_q^+ = I_q^+{}_{GC}$ = 5.14 A), but considering P_G = 1.4 kW (medium-production scenario). Observe that $I_p^+ = I_p^+{}_{max}$ = 7.06 A to avoid exceeding the inverter rated current, therefore active power curtailment is performed (from 1.4 kW to 1 kW). As shown in Fig. 9(e) and (f), the current injected by the VSI reaches the maximum allowed value without exceeding I_{rated}, avoiding active power oscillations.

E. Case 5: Severe Grid Fault Conditions. Only Q Injection

Fig. 10 shows the system in LVRT operation ($V^+ < 0.5$ p.u.) considering P_G = 1.4 kW (medium-production scenario). Hence, with V^+ = 0.45 p.u., and according to (5), the VSI has to inject a minimum reactive current $I_q^+ = I_q^+{}_{GC}$ = 9 A, but with this value, a total active power curtailment is performed during the sag ($I_p^+{}_{max} = I_p^+ = I_p^-$ = 0). Furthermore, because of the unbalanced fault (V^- = 0.05 p.u.), the VSI also injects a negative-sequence reactive current I_q^- = 1 A. Looking at Fig. 10(e) and (f), it is evident that the injected currents (i_{abc}) have been limited to the safe operation value of the inverter, and that the active power is free from oscillations during the voltage sag ($0.1 < t < 0.4$ s). From the data in Fig. 3(a), it is clear that under a voltage fault with the same characteristics but a balanced one (V^- = 0), it would be possible to inject some amount of active power (approximately 458 W). In this

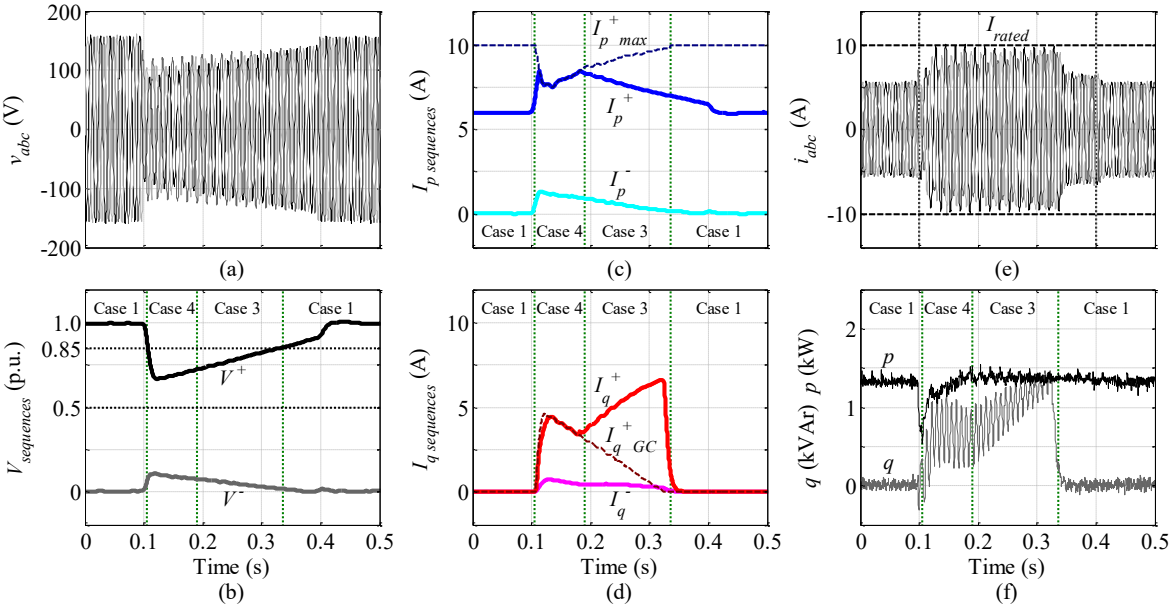

Fig. 12. Experimental results with a variable-profile voltage sag. (a) Phase voltages. (b) Voltage sequences. (c) Active current sequences. (d) Reactive current sequences. (e) Phase currents. (f) Measured powers.

case, it would be equivalent to injecting a current $I_p^+ = 4.36$ A.

It is important to note that the real-time detection of the voltage sequence components presents a delay, due to the sequence extractor [44], and with such an abrupt change in the active power injection (at $t = 0.4$ s), slight overshoot and oscillation are noticeable while reaching steady state (pre-fault value).

F. Case 6: Severe Grid Fault Conditions. Only Positive Q Injection

Fig. 11 shows the system in LVRT operation ($V^+ < 0.5$ p.u.) considering $P_G = 1.4$ kW (medium-production scenario) and with a fault even more unbalanced, $V^+ = 0.40$ p.u. and $V^- = 0.17$ p.u. According to (5), the VSI has to inject into the grid a minimum reactive current $I_q^+ = I_q^+{}_{GC} = 9$ A, but with this value of I_q^+, a total active power curtailment is mandatory ($I_p^+{}_{max} = I_p^+ = I_p^- = 0$). Also, due to the magnitude of V^-, the value of I_{rated} is exceeded, and consequently the inverter can only inject positive-sequence reactive current ($I_q^+ = 10$ A) to comply with the maximum injection and RCI requirements. Fig. 11(e) and (f) reveals that the injected currents are balanced, that the proposed method limits the peak current to the predefined value $I_{rated} = 10$ A, and also, that the peak value of active power ripple is 430 W. It must be noted that only in the case of the most severe sag, objective 4 is not accomplished.

G. Supporting Dynamic Voltage Sags

Finally, a dynamic laboratory test has been carried out to further demonstrate the effectiveness of the proposed control strategy under a variable-profile voltage sag, as shown in Fig. 12. Both the test and the sag have the time behavior previously described, i.e., the sag occurs from $t = 0.1$ s to $t = 0.4$ s.

It is worth noting that although the voltage disturbance extends for 0.3 s, in the interval $0.1 < t < 0.4$ s, the maximum current injection and RCI (I_q^+ and I_q^-) only occur during 0.23 s, in the interval $0.11 < t < 0.34$ s, i.e., while $V^+ < 0.85$ p.u. Note that as the voltage is restored and the V^+ value increases, the amplitudes of I_p^+ and I_p^- decrease to keep the power flow set-point. This dynamic can be seen from $t = 0.18$ s.

H. Discussion on the Benefits of the Proposed Strategy

Table V presents a comparison between the most representative strategies and the proposal made in the present study. It should be noted that the proposed strategy aims to achieve four control objectives at the same time, not independently. Also, the level of complexity of this control scheme is lower compared to other approaches despite the fact that it explores a larger number of possible cases. The proposed strategy prioritizes reactive power injection to accomplish the current requirements of GCs. Reference currents are calculated online according to the amplitude of the positive-sequence voltage V^+.

About the control of active power, it will be assumed that there is no control of this power during the fault if a certain value has been previously set or if it has been established to zero and, consequently, the controller cannot change this condition during the sag. It should be mentioned that the proposal incorporates a current amplitude limitation control (CALC) as an essential part of its control strategy. In this sense, the algorithm is strict when establishing the maximum current value as $I_{max} = I_{rated}$, as in [29]. In [27] $I_{max} = 1.4\ I_{rated}$, and in [31] $I_{max} = 1.2\ I_{rated}$, which makes the current amplitude control less restrictive.

The current control proposal also involves mitigation of active power oscillations, as already explained, which is an important and desirable characteristic. In [31], the same author acknowledges that his "method cannot operate at zero active power ripple operation" when it only injects reactive current. The method mentioned above does not exceed I_{max} but it is not able to avoid the active power ripple, it only limits it. On the contrary, case five of this research shows that active power oscillations can be avoided, even if only reactive power is injected under the same conditions (the voltage sag severity

TABLE V
COMPARISON WITH PREVIOUS STRATEGIES

	Objective 1		Objective 2	Objective 3	Objective 4		
Strategy	RCI for LVRT	Grid Code	CALC	Active Power Control	zero *p* oscillation	Injection	Studied Cases
[25], 2010	yes	no	yes	no	no	Q	3
[24], 2011	yes	no	yes	no	no	Q	2
[27], 2011	yes	yes	yes	yes	no	P and Q	2
[20], 2013	yes	no	yes	yes	no	P and Q	3
[21], 2013	yes	no	no	no	no	P and Q	2
[22], 2014	yes	no	yes	no	no	Q	2
[28], 2015	yes	no	yes	yes	no	P and Q	2
[29], 2016	no	no	yes	yes	yes	P and Q	3
[31], 2016	yes	yes	yes	yes	not always	P and Q	2
Proposal	yes	yes	yes	yes	yes	P and Q	6

will determine the most suitable control action). All these properties together allow the grid to be supported and, at the same time, extend the life of the inverter-based DPGS.

The Spanish GC has been selected as the reference GC to carry out all the tests taking into account the required RCI ratio (I_q^+ / I_{rated}). However, any GC could be taken as a reference and could be introduced into the algorithm by changing (5). Other studies have used more than one GC to perform their tests, thus obtaining part of their experimental results under the regulation of a GC and the other part of the results with the regulation of another GC. The GCs of Denmark and Germany are used by [27], and the GCs of Germany and Spain are used by [31].

In the literature, most papers discuss two or three injection scenarios, but more are needed in practice; in this sense, more voltage sags must also be considered. In addition, real/practical voltage sags have a dynamic profile; however, the performance of several control strategies is not tested in this realistic scenario.

Finally, the dynamic behavior of the control strategy is remarkable. It allows getting smooth transitions under various power conditions and also during the changes between the different cases (operational modes), as seen in Fig. 12. After the grid failure has been cleared, the inverter can quickly achieve its normal operation, as shown by the experimental results.

V. CONCLUSION

Although extensive research has been carried out on control strategies of inverter-based DPGSs, most studies on this issue have been conducted with a reduced number of control objectives. Moreover, little attention has been paid to the relationship between the minimum reactive current and the maximum active current that can be injected into the grid when a voltage sag occurs. This paper has presented an improved LVRT control strategy that maximizes the power delivery capabilities of the inverter-based DPGS under voltage sags. The effectiveness of the proposed control strategy has been validated by a broad set of experimental results, which demonstrate the fulfillment of the proposed control objectives:

1. To meet LVRT and RCI requirements defined in current GCs.
2. To limit the amount of injected current to the maximum allowed by the inverter.
3. Active power control in normal operation and under grid voltage sags.
4. To avoid active power oscillations.

All these control objectives contribute to improve the stability of the network and ensure an optimum use of the entire power capability of the inverter. Although the fourth goal is compromised when only I_q^+ is injected into the grid, the first three control objectives are always achieved. Also, different power levels and different voltage sag profiles are considered. As a result, three main operational modes have been identified: active power injection, active and reactive power injection, and reactive power injection. In the first mode, the maximum current injection can be achieved by supplying only active power. In the second one, both active and reactive power will be injected to reach the maximum rated current of the inverter and to provide support to the grid during the fault. In the third one, the maximum current injection can be achieved by providing only reactive power.

The new scenario of standardization and GCs, restrictive in some cases, has to be widely incorporated into new control strategies with more sophisticated algorithms and schemes that allow satisfying a higher number of control objectives.

REFERENCES

[1] "CIGRE (Conseil International des Grands Réseaux Electriques)," *The World Forum for Power Systems*, 2016. [Online]. Available: www.cigre.org.

[2] F. Blaabjerg, R. Teodorescu, M. Liserre, and A. V. Timbus, "Overview of Control and Grid Synchronization for Distributed Power Generation Systems," *IEEE Trans. Ind. Electron.*, vol. 53, no. 5, pp. 1398–1409, Oct. 2006.

[3] M. Tsili and S. Papathanassiou, "A review of grid code technical requirements for wind farms," *IET Renew. Power Gener.*, vol. 3, no. 3, p. 308, 2009.

[4] M. Altin, O. Goksu, R. Teodorescu, P. Rodriguez, B.-B. Jensen, and L. Helle, "Overview of recent grid codes for wind power integration," in *2010 12th International Conference on Optimization of Electrical and Electronic Equipment*, 2010, pp. 1152–1160.

[5] Y. Yang, P. Enjeti, F. Blaabjerg, and H. Wang, "Wide-Scale Adoption of Photovoltaic Energy: Grid Code Modifications Are Explored in the Distribution Grid," *IEEE Ind. Appl. Mag.*, vol. 21, no. 5, pp. 21–31, Sep. 2015.

[6] "Waveform Characteristics of Voltage Sags: Statistical Analysis. TR-112692," EPRI, Palo Alto, CA, 1999.

[7] *IEEE Recommended Practice for Monitoring Electric Power Quality*. IEEE Std 1159™-2009 (Revision of IEEE Std 1159-1995), 2009.
[8] R. Teodorescu, M. Liserre, and P. Rodríguez, "Grid Requirements for PV," in *Grid Converters for Photovoltaic and Wind Power Systems*, Chichester, UK: John Wiley & Sons, Ltd, 2010, pp. 31–42.
[9] R. Teodorescu, M. Liserre, and P. Rodríguez, "Grid Requirements for WT Systems," in *Grid Converters for Photovoltaic and Wind Power Systems*, Chichester, UK: John Wiley & Sons, Ltd, 2010, pp. 145–167.
[10] C. Sourkounis and P. Tourou, "Grid Code Requirements for Wind Power Integration in Europe," *Conf. Pap. Energy*, vol. 2013, pp. 1–9, 2013.
[11] *Network Code for Requirements for Grid Connection Applicable to all Generators*. ENTSO-E, 2013.
[12] *Grid Code for high and extra high voltage*. E.ON Netz GmbH, 2006.
[13] *P.O. 12.3. Requisitos de respuesta frente a huecos de tensión de las instalaciones eólica*. Red Eléctrica de España (REE), 2006.
[14] "Regulamento da Rede de Transporte," 2010. [Online]. Available: http://www.erse.pt/pt/electricidade/liberalizacaodosector/Paginas/default.aspx.
[15] *Distribution Code*. Distribution System Operator ESB Networks Limited, 2016.
[16] *Commission Regulation (EU) 2016/631 establishing a network code on requirements for grid connection of generators*. The European Commission, 2016.
[17] J. L. Blackburn and T. J. Domin, "Symmetrical Components: A Review," in *Protective Relaying: Principles and Applications*, Third Edit., CRC Press, 2006.
[18] S. Alepuz, S. Busquets-Monge, J. Bordonau, J. A. Martinez-Velasco, C. A. Silva, J. Pontt, and J. Rodriguez, "Control Strategies Based on Symmetrical Components for Grid-Connected Converters Under Voltage Dips," *IEEE Trans. Ind. Electron.*, vol. 56, no. 6, pp. 2162–2173, Jun. 2009.
[19] Fei Wang, J. L. Duarte, and M. A. M. Hendrix, "Pliant Active and Reactive Power Control for Grid-Interactive Converters Under Unbalanced Voltage Dips," *IEEE Trans. Power Electron.*, vol. 26, no. 5, pp. 1511–1521, May 2011.
[20] A. Camacho, M. Castilla, J. Miret, J. C. Vasquez, and E. Alarcon-Gallo, "Flexible Voltage Support Control for Three-Phase Distributed Generation Inverters Under Grid Fault," *IEEE Trans. Ind. Electron.*, vol. 60, no. 4, pp. 1429–1441, Apr. 2013.
[21] J. Miret, A. Camacho, M. Castilla, L. G. de Vicuña, and J. Matas, "Control Scheme With Voltage Support Capability for Distributed Generation Inverters Under Voltage Sags," *IEEE Trans. Power Electron.*, vol. 28, no. 11, pp. 5252–5262, Nov. 2013.
[22] A. Camacho, M. Castilla, J. Miret, R. Guzman, and A. Borrell, "Reactive Power Control for Distributed Generation Power Plants to Comply With Voltage Limits During Grid Faults," *IEEE Trans. Power Electron.*, vol. 29, no. 11, pp. 6224–6234, Nov. 2014.
[23] J. Miret, M. Castilla, A. Camacho, L. G. de Vicuña, and J. Matas, "Control Scheme for Photovoltaic Three-Phase Inverters to Minimize Peak Currents During Unbalanced Grid-Voltage Sags," *IEEE Trans. Power Electron.*, vol. 27, no. 10, pp. 4262–4271, Oct. 2012.
[24] P. Rodriguez, A. Luna, J. R. Hermoso, I. Etxeberria-Otadui, R. Teodorescu, and F. Blaabjerg, "Current control method for distributed generation power generation plants under grid fault conditions," in *IECON 2011 - 37th Annual Conference of the IEEE Industrial Electronics Society*, 2011, pp. 1262–1269.
[25] P. Rodriguez, G. Medeiros, A. Luna, M. C. Cavalcanti, and R. Teodorescu, "Safe current injection strategies for a STATCOM under asymmetrical grid faults," in *2010 IEEE Energy Conversion Congress and Exposition*, 2010, pp. 3929–3935.
[26] J. A. Suul, A. Luna, P. Rodríguez, and T. Undeland, "Virtual-Flux-Based Voltage-Sensor-Less Power Control for Unbalanced Grid Conditions," *IEEE Trans. Power Electron.*, vol. 27, no. 9, pp. 4071–4087, Sep. 2012.
[27] C.-T. Lee, C.-W. Hsu, and P.-T. Cheng, "A Low-Voltage Ride-Through Technique for Grid-Connected Converters of Distributed Energy Resources," *IEEE Trans. Ind. Appl.*, vol. 47, no. 4, pp. 1821–1832, Jul. 2011.
[28] A. Camacho, M. Castilla, J. Miret, A. Borrell, and L. G. de Vicuna, "Active and Reactive Power Strategies With Peak Current Limitation for Distributed Generation Inverters During Unbalanced Grid Faults," *IEEE Trans. Ind. Electron.*, vol. 62, no. 3, pp. 1515–1525, Mar. 2015.
[29] J. L. Sosa, M. Castilla, J. Miret, J. Matas, and Y. A. Al-Turki, "Control Strategy to Maximize the Power Capability of PV Three-Phase Inverters During Voltage Sags," *IEEE Trans. Power Electron.*, vol. 31, no. 4, pp. 3314–3323, Apr. 2016.
[30] C. Tang, Y.-T. Chen, and Y. Chen, "PV Power System With Multi-Mode Operation and Low-Voltage Ride-Through Capability," *IEEE Trans. Ind. Electron.*, vol. 62, no. 12, pp. 7524–7533, Dec. 2015.
[31] H.-C. Chen, C.-T. Lee, P.-T. Cheng, R. Teodorescu, and F. Blaabjerg, "A Low-Voltage Ride-Through Technique for Grid-connected Converters with Reduced Power Transistors Stress," *IEEE Trans. Power Electron.*, vol. 31, no. 12, pp. 8562–8571, 2016.
[32] M. Braun, T. Stetz, R. Bründlinger, C. Mayr, K. Ogimoto, H. Hatta, H. Kobayashi, B. Kroposki, B. Mather, M. Coddington, K. Lynn, G. Graditi, A. Woyte, and I. MacGill, "Is the distribution grid ready to accept large-scale photovoltaic deployment? State of the art, progress, and future prospects," *Prog. Photovoltaics Res. Appl.*, vol. 20, no. 6, pp. 681–697, Sep. 2012.
[33] Y. Xue, K. C. Divya, G. Griepentrog, M. Liviu, S. Suresh, and M. Manjrekar, "Towards next generation photovoltaic inverters," in *2011 IEEE Energy Conversion Congress and Exposition*, 2011, pp. 2467–2474.
[34] H. Slootweg, "Smart Grids - the future or fantasy?," in *IET Seminar Digests*, 2009, pp. 10–10.
[35] *IEEE Application Guide for IEEE Std 1547™, IEEE Standard for Interconnecting Distributed Resources with Electric Power Systems*. IEEE Std 1547.2-2008, 2009.
[36] J. Liu, L. Zhou, X. Yu, B. Li, and C. Zheng, "Design and analysis of an LCL circuit-based three-phase grid-connected inverter," *IET Power Electron.*, vol. 10, no. 2, pp. 232–239, Feb. 2017.
[37] *IEEE Recommended Practice for Electric Power Distribution for Industrial Plants*. IEEE Std 141™-1993 (R1999), 1994.
[38] P. Pillay and M. Manyage, "Definitions of Voltage Unbalance," *IEEE Power Eng. Rev.*, vol. 21, no. 5, pp. 49–51, 2001.
[39] G. Lammert, T. Hes, M. Schmidt, P. Schegner, and M. Braun, "Dynamic Grid Support in Low Voltage Grids–Fault Ride-Through and Reactive Power/Voltage Support during Grid Disturbances," in *2014 Power Systems Computation Conference*, 2014, pp. 1–7.
[40] R. Teodorescu, M. Liserre, and P. Rodríguez, "Control of Grid Converters under Grid Faults," in *Grid Converters for Photovoltaic and Wind Power Systems*, Chichester, UK: John Wiley & Sons, Ltd, 2010, pp. 237–287.
[41] A. Yazdani and R. Iravani, "Space Phasors and Two-Dimensional Frames," in *Voltage-Sourced Converters in Power Systems*, Hoboken, NJ, USA: John Wiley & Sons, Inc., 2010, pp. 69–114.
[42] F. J. Rodriguez, E. Bueno, M. Aredes, L. G. B. Rolim, F. A. S. Neves, and M. C. Cavalcanti, "Discrete-time implementation of second order generalized integrators for grid converters," in *2008 34th Annual Conference of IEEE Industrial Electronics*, 2008, no. 1, pp. 176–181.
[43] D. N. Zmood, D. G. Holmes, and G. H. Bode, "Frequency-domain analysis of three-phase linear current regulators," *IEEE Trans. Ind. Appl.*, vol. 37, no. 2, pp. 601–610, 2001.
[44] J. Matas, M. Castilla, J. Miret, L. Garcia de Vicuna, and R. Guzman, "An Adaptive Prefiltering Method to Improve the Speed/Accuracy Tradeoff of Voltage Sequence Detection Methods Under Adverse Grid Conditions," *IEEE Trans. Ind. Electron.*, vol. 61, no. 5, pp. 2139–2151, May 2014.

Miguel A. Garnica L. was born in San Juan de Pasto, Nariño, Colombia, in December 1973. He received the B.S. in naval engineering from Escuela Naval de Cadetes "Almirante Padilla", Cartagena de Indias, Colombia, in 2002 and the M.S. degree in electronic engineering from the University of Barcelona, Barcelona, Spain, in 2012.

He is currently working toward the Ph.D. degree in the Department of Electronic Engineering, Technical University of Catalonia, Spain. His research interests include power electronics, control systems, and renewable energy systems.

Luis García de Vicuña received the M.S. and Ph.D. degrees in Telecommunication Engineering from the Technical University of Catalonia, Barcelona, Spain, in 1980 and 1990, respectively, and the Ph.D. degree in Electrical Engineering from the Paul Sabatier University, Toulouse, France, in 1992.

He is currently a Full Professor with the Department of Electronic Engineering, Technical University of Catalonia, where he teaches courses on power electronics. His research interests include power electronics modeling, simulation and control, active power filtering, and high power-factor ac/dc conversion.

Jaume Miret (M'98) received the B.S. degree in telecommunications, M.S. degree in electronics, and Ph.D. degree in electronics from the Universitat Politècnica de Catalunya, Barcelona, Spain, in 1992, 1999, and 2005, respectively.

From 1993 to 2011, he was an Assistant Professor in the Department of Electronic Engineering, Universitat Politècnica de Catalunya, Spain. Since 2011 he has been an Associate Professor in the Universitat Politècnica de Catalunya, where he teaches courses on digital design and circuit theory. His research interests include dc-to-ac converters, active power filters, and digital control.

Miguel Castilla received the B.S., M.S. and Ph.D. degrees in telecommunication engineering from the Technical University of Catalonia, Barcelona, Spain, in 1988, 1995, and 1998, respectively.

Since 2002, he has been an Associate Professor in the Department of Electronic Engineering, Technical University of Catalonia, where he teaches courses on analog circuits and power electronics. His research interests are in the areas of power electronics, nonlinear control, and renewable energy systems.

Ramón Guzmán received the B.S., the M.S. and the Ph.D. degrees in telecommunications engineering from the Technical University of Catalonia, Barcelona, Spain, in 1999, 2004 and 2016, respectively.

He is currently an Associate Professor with the Department of Automatic Control in the Technical University of Catalonia. His research interests include nonlinear and adaptive control for three-phase power converters.